Journal of Nanobiotechnology

RESEARCH Open Access

Apoptotic metabolites ameliorate bone aging phenotypes via TCOF1/FLVCR1-mediated mitochondrial homeostasis

Yan Qu[1†], Bowen Meng[1†], Simin Cai[1†], Benyi Yang[1], Yifan He[1], Chaoran Fu[1], Xiangxia Li[1], Peiyi Li[1], Zeyuan Cao[1], Xueli Mao[1], Wei Teng[1*] and Songtao Shi[1*]

Abstract

Over 50 billion cells undergo apoptosis each day in an adult human to maintain tissue homeostasis by eliminating damaged or unwanted cells. Apoptotic deficiency can lead to age-related diseases with reduced apoptotic metabolites. However, whether apoptotic metabolism regulates aging is unclear. Here, we show that aging mice and apoptosis-deficient MRL/*lpr* (B6.MRL-Faslpr/J) mice exhibit decreased apoptotic levels along with increased aging phenotypes in the skeletal bones, which can be rescued by the treatment with apoptosis inducer staurosporine (STS) and stem cell-derived apoptotic vesicles (apoVs). Moreover, embryonic stem cells (ESC)-apoVs can significantly reduce senescent hallmarks and mtDNA leakage to rejuvenate aging bone marrow mesenchymal stem cells (MSCs) and ameliorate senile osteoporosis when compared to MSC-apoVs. Mechanistically, ESC-apoVs use TCOF1 to upregulate mitochondrial protein transcription, resulting in FLVCR1-mediated mitochondrial functional homeostasis. Taken together, this study reveals a previously unknown role of apoptotic metabolites in ameliorating bone aging phenotypes and the unique role of TCOF1/FLVCR1 in maintaining mitochondrial homeostasis.

Keywords Apoptosis, Apoptotic vesicles, Senile osteoporosis, Mitochondrial homeostasis

Introduction

Over 50 billion cells undergo apoptosis each day in an adult human, which plays a pivotal role in the maintenance of tissue homeostasis and eliminating damaged or unwanted cells [1, 2]. Accumulating experimental evidence has shown that apoptotic disorders can lead to a variety of anomalies, including aging, autoimmune diseases and cancer [3, 4]. Senescent cells are resistant to apoptosis, leading to the accumulation of senescent cells and further exacerbating the aging process. Recent studies show that apoptotic cells can release metabolites to exert certain physiological functions [5]. However, whether apoptotic metabolites regulate senile osteoporosis remains unclear.

†Yan Qu, Bowen Meng and Simin Cai contributed equally to this work.

*Correspondence:
Wei Teng
tengwei@mail.sysu.edu.cn
Songtao Shi
shisongtao@mail.sysu.edu.cn
[1]Hospital of Stomatology, Guanghua School of Stomatology, South China Center of Craniofacial Stem Cell Research, Guangdong Provincial Key Laboratory of Stomatology, Sun Yat-sen University, Guangzhou 510055, China

Apoptotic vesicles (apoVs) are a specific type of extracellular vesicles (EVs) released during apoptosis, which are critical for maintaining organ and body homeostasis [5, 6]. Previous studies have shown that apoptotic vesicles can regulate immune response, promote DNA damage repair, enhance skin wound healing and hair regeneration, and effectively treat multiple myeloma and other diseases [5, 7–10]. Our previous study found that mesenchymal stem cells (MSCs)-derived apoptotic vesicles can treat osteoporosis in ovariectomy-induced mice [5]. Compared with MSCs, embryonic stem cells (ESCs) are renowned for their more excellent pluripotency and stemness [11, 12]. Our previous studies found that the apoVs derived from ESCs inherit many characteristics of their parent cells, and ESC-apoVs demonstrate greater regenerative and reparative potential [7]. However, whether ESC-apoVs can be used as a more effective EVs to treat senile osteoporosis (SOP) remains unclear.

Mitochondrial dysfunction is one of the hallmarks of aging [13–15]. Several factors are demonstrated to trigger the decline of mitochondrial function during aging, including elevated ROS production, mitochondrial DNA (mtDNA) mutations, protein oxidations, abnormal energy metabolism, and reduced mitochondrial biogenesis [16–18]. Recent studies have shown senescent cells release mitochondrial DNA (mtDNA) into the cytoplasm [19, 20], which exacerbates the senescence-associated secretory phenotype (SASP) to promote the aging process [20, 21]. This suggests that maintaining mitochondrial homeostasis may be a potential treatment for age-related diseases.

This study demonstrates that apoptosis and apoptotic metabolites are required to maintain bone homeostasis in senile osteoporosis. In addition, we found that ESC-apoVs inherit TCOF1 from their parent cells, which upregulates mitochondrial protein transcription of FLVCR1 to maintain mitochondrial functional homeostasis.

Results

Apoptosis is required to attenuate the accumulation of senescent cells and ameliorate senile osteoporosis

Previous studies have shown that aging mice are resistant to apoptosis [22], but it is unclear whether reduced apoptosis levels will exacerbate osteoporosis. TUNEL staining and tissue immunofluorescence results showed that the femur of aging mice exhibited significant reduced apoptosis rate and apoptotic hallmarks cleaved caspase 3 compared to young mice (Fig. 1A). We utilized P21 and β-Gal staining to assess senescent cells in tissues. Immunofluorescence and SA-β-Gal staining results showed that the femurs of aging mice exhibited significant upregulation of aging hallmarks, including γH2AX, P21 and SA-β-Gal, and downregulation of proliferation markers, such as PCNA, compared to young mice. (Fig. 1B). Alizarin red staining and Oil Red O staining results showed that the bone marrow mesenchymal stem cells (BMMSCs) of aging mice exhibited decreased osteogenic differentiation ability and increased adipogenic differentiation ability (Fig. 1C and D). The results of micro-CT showed that aging mice exhibited the osteoporosis phenotype, as evidenced by decreased bone mineral density (BMD), bone volume/tissue volume (BV/TV) and trabecular number (Tb.n) (Fig. 1E and F). Therefore, we speculate that apoptosis resistance in the femur may be a key factor causing femoral bone aging. Abnormalities in endogenous and exogenous apoptosis signaling pathways can lead to apoptosis resistance of senescent cells in aging mice [22, 23]. Fas is a vital molecule in the exogenous apoptotic pathway. Our recent study showed that six-month-old Fas^{mut} mice exhibited premature senescence [10]. To further confirm the relationship between apoptosis resistance and SOP, we analyzed aging and apoptosis levels in the bone marrow of six-month-old apoptosis-deficient (Fas^{mut}) mice. The results showed that apoptosis-deficient mice showed decreased apoptosis rate, accompanied by increased aging levels and adipogenic differentiation ability, and decreased osteogenic differentiation ability, proliferation ability and bone parameters compared to wild-type mice (Figure S1A-E). The above results confirm that apoptosis resistance can cause bone aging phenotypes.

Next, we investigate whether increasing apoptosis level can rescue the osteoporosis phenotype in aging mice. We utilized a well-known apoptosis inducer staurosporine to induce apoptosis *via* activation of both endogenous and exogenous pathways [24]. STS was intraperitoneally administered to mice twice a week for 8 weeks. The results showed that STS treatment effectively increased trabecular BMD, BV/TV, and Tb.n of the femurs. It also enhanced osteogenic differentiation ability and reduced adipogenic differentiation ability in aging mice. This was accompanied by a significant upregulation of apoptosis level, proliferation ability, and a decrease in the level of aging hallmarks (Fig. 1A-F)). Our previous study showed that staurosporine elevated apoptosis in vivo and rescued impaired MSCs in Fas^{mut} mice [5]. Similarly, STS treatment increased the osteogenic differentiation ability and decreased the adipogenic differentiation ability of Fas^{mut} BMMSCs. This was accompanied by a significant upregulation of apoptosis levels, proliferation ability and bone parameters, as well as a decrease in the level of aging hallmarks (Figure S1A-E). These data suggest that increased apoptotic level attenuates the accumulation of senescent cells and rescues senile osteoporosis.

ESC-apoVs significantly ameliorate bone aging phenotypes

We further examined the changes in endogenous apoptotic vesicle levels in the femur and serum of aging mice

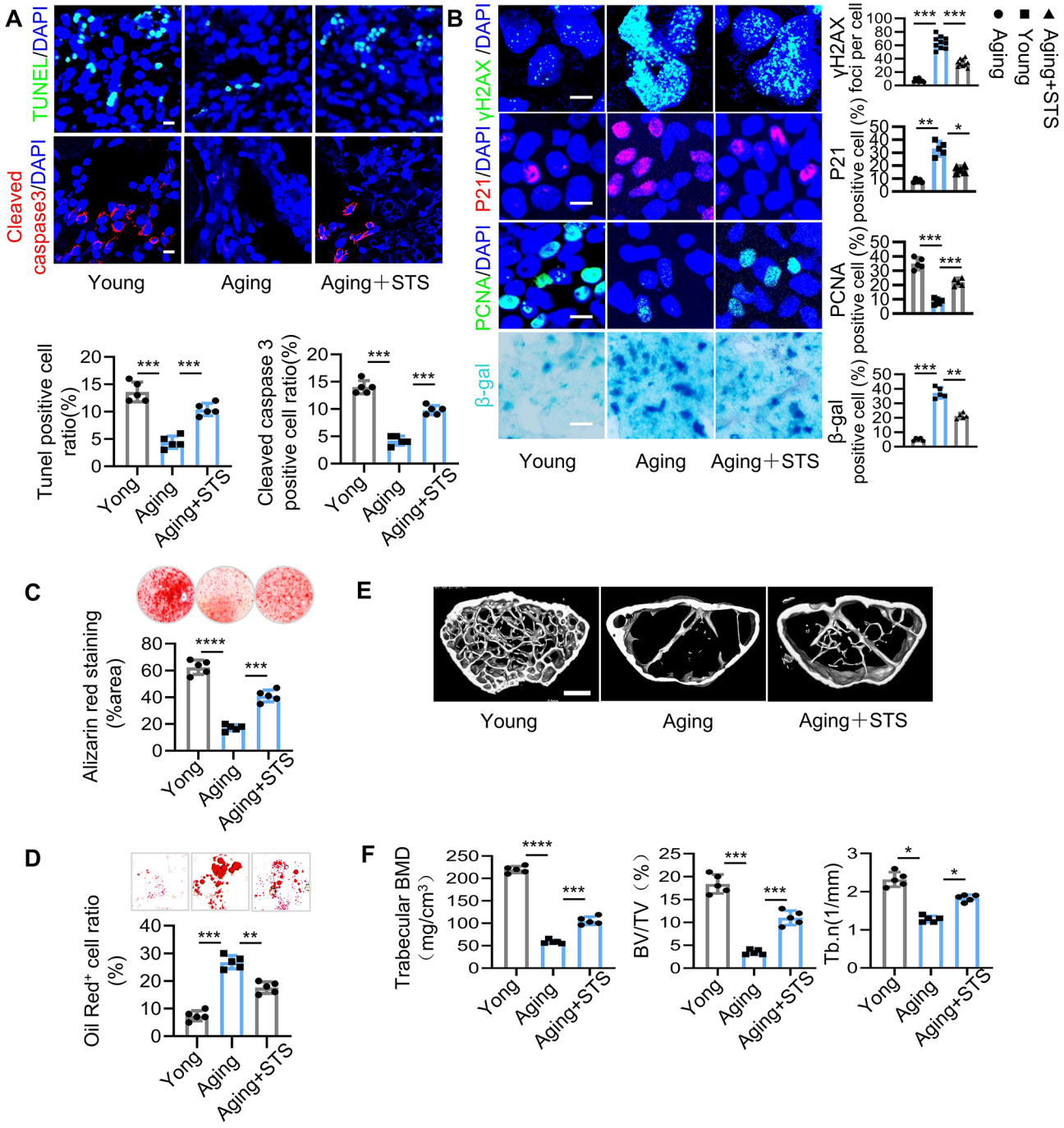

Fig. 1 Increased apoptotic metabolism rescues senile osteoporosis *via* attenuating senescent cell accumulation. **(A)** TUNEL staining (green) and immunofluorescence images of cleaved caspase3 (red) showed apoptosis of bone marrow cells in aging mice. Scale bar, 10 μm. ($n=5$). **(B)** Immunofluorescent images (left) and semi-quantification (right) of γH2AX foci ($n=10$), P21, PCNA and β-Gal ($n=5$) in aging mouse bone marrow. Scale bar, 20 μm (up) and 10 μm (down). **(C)** Osteogenesis of BMMSCs in aging mice as assessed by Alizarin red staining ($n=5$). **(D)** Adipogenesis of BMMSCs in aging mice as assessed by Oil Red O staining ($n=5$). **E and F.** MicroCT images and analysis of the distal femurs in aging mice. Scale bar, 0.5 mm ($n=5$). Data were analyzed by one-way ANOVA with Bonferroni test for comparison of multiple groups. *$p<0.05$, **$p<0.01$, ***$p<0.001$, and ****$p<0.0001$

following our previously reported methods [5]. Western blot and nanoflow cytometry results showed that apoVs derived from the circulation and femur of *Fas*^{mut} mice expressed apoV-specific markers cleaved caspase3 along with exosome-associated proteins CD9 and TSG101 (Figures S1F-H). TEM and Elyra 7 Lattice SIM analysis showed that apoVs derived from the circulation and femur of *Fas*^{mut} mice were a double-layered vesicle-like structure (Figure S1I, S1J). NTA results showed that the circulation and femur in *Fas*^{mut} mice exhibited reduced

levels of endogenous apoptotic vesicles compared to WT mice, which were rescued by STS treatment (Figure S1K). The above results suggest that endogenous apoptotic vesicle levels are reduced in *Fas*^{mut} mice, but this reduction can be reversed by STS treatment.

To further explore the potential relationship between the reduction of apoVs and the senescence phenotypes in SOP, we examined whether recipient BMMSCs engulf apoVs after apoV-infusion. Immunofluorescent staining showed that PKH26-labeled apoVs could be detected in CD90-positive BMMSCs in the bone marrow of WT mice after 24 h tail vein injection, as reported previously [7]. (Fig. 2A). Our previous studies confirmed that ESC-derived apoptotic vesicles can empower MSCs to improve their osteogenic function [7]. Therefore, we further explored whether ESC-apoVs could restore the osteogenic function of aging BMMSCs and treat SOP in vivo. We intravenously infused 1.6×10^{10} of ESC-apoVs, umbilical mesenchymal stem cell (UMSC)-apoVs or PBS per mouse twice a week for two consecutive months. The results of micro-CT showed that ESC-apoV treatment effectively increased BV/TV, trabecular BMD and trabecular number (Tb.n) in the femur of aging mice compared to UMSC-apoVs and PBS groups (Fig. 2B). TRAP/ALP staining revealed that ESC-apoV treatment showed a significant increase in ALP-positive cells and a significant decrease in TRAP-positive cells compared to UMSC-apoVs and PBS groups (Fig. 2C). This indicates that ESC-apoV treatment increased the number of ALP$^+$ osteoblasts and decreased the number of TRAP$^+$ osteoclasts in the femur of aging mice.

Following the ESC-apoV treatment, the femur of aging mice showed significant upregulated apoptosis level, as assessed by TUNEL staining (Fig. 2D and E). In vivo animal imaging results showed that ESC-apoV treatment effectively reduced the fluorescence levels of mice femurs in P16 fluorescently labeled mice compared to UMSC-apoVs and PBS groups (Fig. 2F). ESC-apoV treatment significantly decreased aging markers, including the number of γH2AX foci, P21 and SA-β-Gal positivity rate, and increased proliferation markers, such as PCNA in the bone marrow compared to UMSC-apoVs and PBS groups (Fig. 2G). ELISA analysis revealed that ESC-apoV treatment significantly decreased the levels of SASP-related factors IL-6, IL-8, MCP-1, and TNF-α, compared to UMSC-apoVs and PBS groups (Fig. 2H). Since mitochondrial DNA (mtDNA) release plays a crucial role in driving the senescence process [19, 20, 25], we examined whether apoVs could mitigate the release of mtDNA from myeloid cells. qPCR analysis revealed that ESC-apoV treatment significantly decrease mtDNA release compared to UMSC-apoVs and PBS groups (Fig. 2I). This indicates that ESC-apoVs facilitate bone formation by decreasing senescence phenotypes in SOP.

Furthermore, we co-cultured aging BMMSCs with ESC-apoVs or UMSC-apoVs for 24 h in vitro. Immunofluorescent staining showed aging BMMSCs were able to engulf PKH26-labeled apoVs (Fig. 3A). ESC-apoV treatment effectively decreased the levels of cellular senescence markers, including γH2AX, P16, P21 and SA-β-Gal, and increased the level of proliferation markers, such as PCNA, compared with UMSC-apoVs and PBS groups (Fig. 3B and C, Figure S2A, S2B). ESC-apoV treatment exhibited a potent function in promoting osteogenic differentiation but reduced adipogenic differentiation ability compared to UMSC-apoVs and PBS groups (Fig. 3D-G). ELISA analysis revealed that ESC-apoV-treated BMMSCs exhibited significantly decreased levels of SASP-related factors including IL-6, IL-8, MCP-1, and TNF-α, compared to UMSC-apoVs and PBS (Fig. 3H). qPCR analysis revealed that ESC-apoV treatment significantly decrease mtDNA release from aging BMMSCs compared to UMSC-apoVs and PBS groups (Fig. 3I). These data indicate that the exogenous supplement of ESC-apoVs can significantly decrease age-related hallmarks and alleviate senile osteoporosis in aging mice.

ESC-apoVs maintains MSC mitochondrial homeostasis by upregulating mitochondrial protein transcription

Since mitochondrial dysfunction is one hallmark of aging [26, 27], we examined mitochondrial morphological and functional changes to evaluate the impact of ESC-apoVs in aging BMMSCs. TEM and immunofluorescent staining analysis revealed alterations in mitochondrial ultrastructure, including mitochondrial swelling and cristae disorder, along with significant depolarization of mitochondrial membranes in aging BMMSCs. These abnormalities were significantly reversed after ESC-apoV treatment when compared with UMSC-apoVs and PBS groups (Fig. 4A and B). Due to the leakage of mtDNA into the cytoplasm, it triggers innate immunity and accelerates the aging process [19–21], we examined mtDNA leakage. Dual immunostaining of TOM20 and DNA revealed that aging BMMSCs contained plenty of DNA nucleoids in the cytosol, as evidenced by increased non-colocalized DNA nucleoli. ESC-apoV treatment significantly reduced the number of DNA nucleoli in the cytoplasm compared with UMSC-apoVs and PBS groups (Fig. 4C and D). The results consistent with the changes in cytoplasmic mtDNA presented in Fig. 3I. These data indicate that ESC-apoVs decreased the release of mtDNA in aging BMMSCs to attenuate SOP.

To determine the mechanism by which ESC-apoVs affect aging BMMSCs, we conducted RNA sequencing analysis of ESC-apoV-treated aging BMMSCs. The results showed 176 differentially expressed genes (DEGs) in ESC-apoV-treated aging BMMSCs compared to control aging BMMSCs, consisting of 73 up-regulated genes

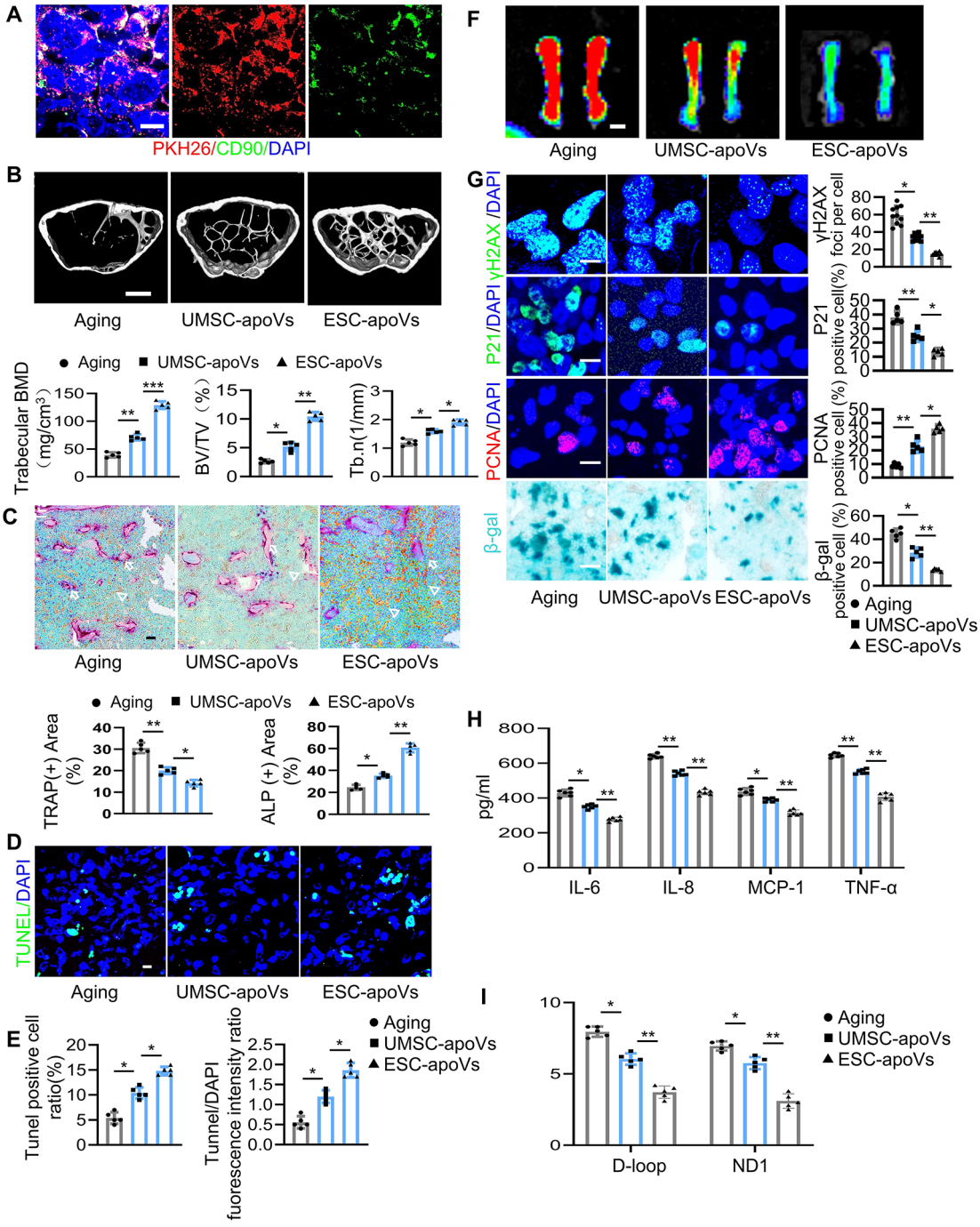

Fig. 2 ESC-apoVs ameliorate senile osteoporosis and reduce age-related hallmarks. **(A)** Representative confocal microscopy images showed the distribution of PKH26-labeled apoVs (red) in the bone marrow 24 h after infusion, DAPI (blue) and CD90 (green) are counterstained. Scale bars, 10 μm. **(B)** MicroCT images and analysis of the distal femurs in aging mice. Scale bars, 0.5 mm ($n = 5$). **(C)** ALP&TRAP double staining of mice femurs. White arrow: TRAP positive cells, White triangle: ALP positive cells. Scale bar: 10 μm. **D and E.** TUNEL staining and statistical analysis showed apoptosis of bone marrow cells. Scale bar, 10 μm ($n = 5$). **F.** Representative images of LUC activity of P16 fluorescence in mouse femurs. Scale bar, 2 μm ($n = 3$). **G.** Semi-quantification of immunofluorescence images of γH2AX foci ($n = 10$), P21, PCNA and β-Gal ($n = 5$) in mouse bone marrow. Scale bar, 20 μm (up) and 10 μm (down). **H.** The expression of SASP factors in aging mice treated with apoVs ($n = 5$). **I.** qPCR analysis of mtDNA release in bone marrow cells ($n = 5$). The cytosol fraction was purified for qPCR analysis of mtDNA and nuclear DNA (nDNA). Two qPCR primers corresponding to the D-loop and ND-1 regions of mtDNA were used. Error bars are mean ± SD. Data were analyzed by one-way ANOVA with Bonferroni test for comparison of multiple groups. *$p < 0.05$, **$p < 0.01$, and ***$p < 0.001$

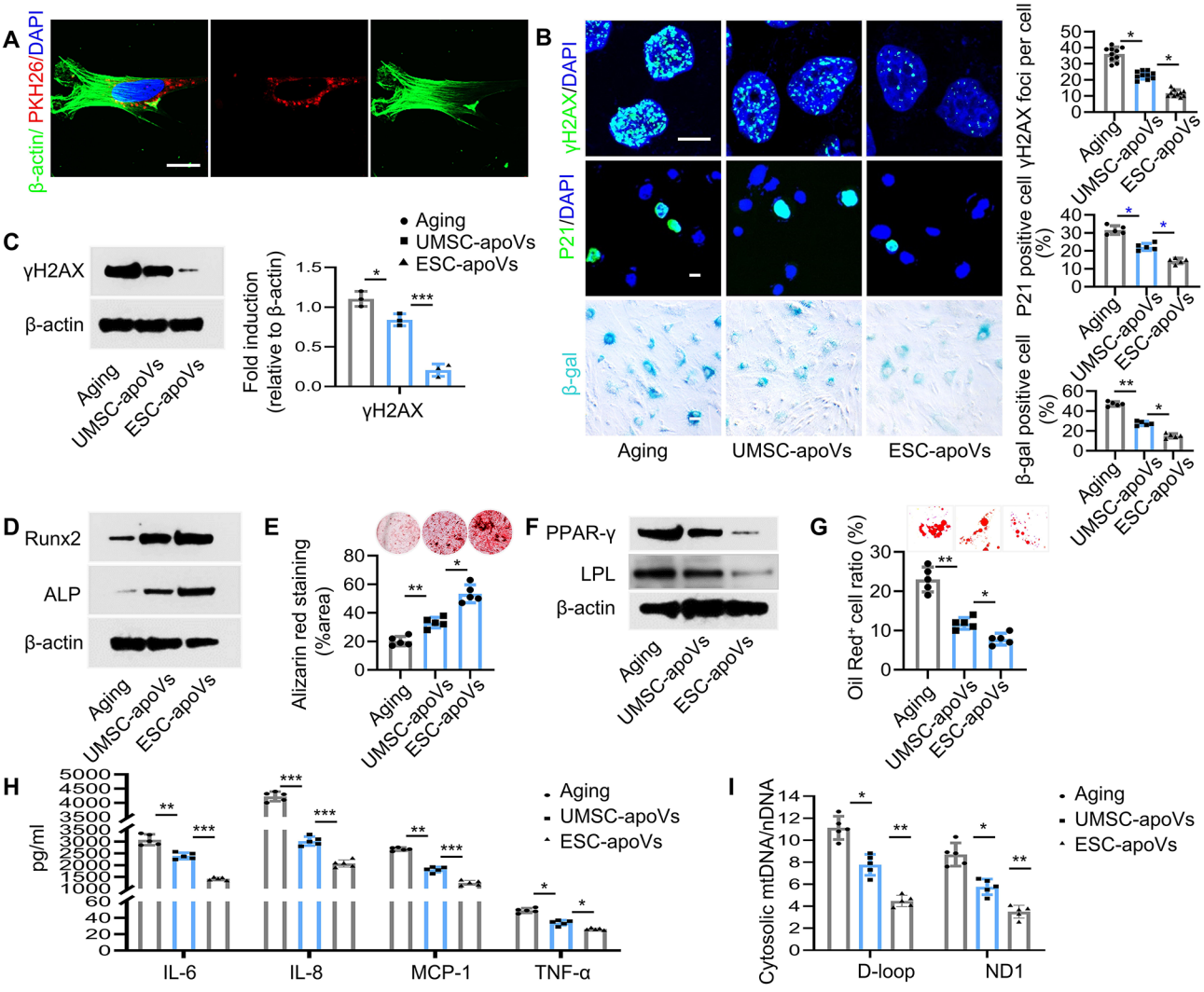

Fig. 3 ESC-apoVs significantly alleviates BMMSCs senescence in vitro. **(A)** PKH26-labeled apoVs were internalized by aging BMMSCs. Scale bar, 5 μm. **(B)** Immunofluorescent images (left) and semi-quantification (right) of γH2AX foci (n = 10), P21 and β-Gal (*n* = 5) of aging BMMSCs with apoVs or PBS treatment. Scale bar, 10 μm. **(C)** Western blot showed expression of senescence marker γH2AX (*n* = 3). **D**, **E.** Osteogenesis of aging BMMSCs was assessed by western blot (*n* = 3) and Alizarin red staining (*n* = 5). **F**, **G.** Adipogenesis of aging BMMSCs was assessed by western blot (*n* = 3) and Oil Red O staining (*n* = 5). **H.** The expression of SASPs factors in aging BMMSCs cocultured with apoVs or PBS (*n* = 5). **I.** qPCR analysis of mtDNA release in aging BMMSCs (*n* = 5). The cytosol fraction was purified for qPCR analysis of mtDNA and nuclear DNA (nDNA). Two qPCR primers corresponding to the D-loop and ND-1 regions of mtDNA were used. Error bars are mean ± SD. Data were analyzed by one-way ANOVA with Bonferroni test for comparison of multiple groups. *$p < 0.05$, **$p < 0.01$, and ***$p < 0.001$

and 103 down-regulated genes (Figure S3A). GO enrichment analysis of RNA-seq dataset indicated that 73 upregulated genes in ESC-apoV-treated aging BMMSCs were associated with rRNA processing, mRNA processing, RNA splicing, mRNA splicing, translation and translational initiation domains (Fig. 4E). The data suggested that ESC-apoVs may regulate mitochondrial protein transcription processes. Then, we analyzed mitochondria-related genes and found that ESC-apoV treatment upregulated mitochondria-related genes in BMMSCs (Fig. 4F and Table 1). Then, we used qPCR to verify the top 10 upregulated genes and found that the highest expression gene was FLVCR1 (Fig. 4G, Figure S3B), which was related to mitochondrial structure [28]. Since aberrant mtDNA packaging enhances the expression of a subset of interferon-stimulated genes (ISGs) [21], we analyzed changes in ISGs in BMMSCs and found that with ESC-apoV treatment downregulated the majority of mtDNA stress-induced ISGs in aging BMMSCs compared to control BMMSCs (Fig. 4H). These results suggest that ESC-apoVs maintained mitochondrial homeostasis of aging BMMSCs *via* upregulating mitochondrial protein transcription.

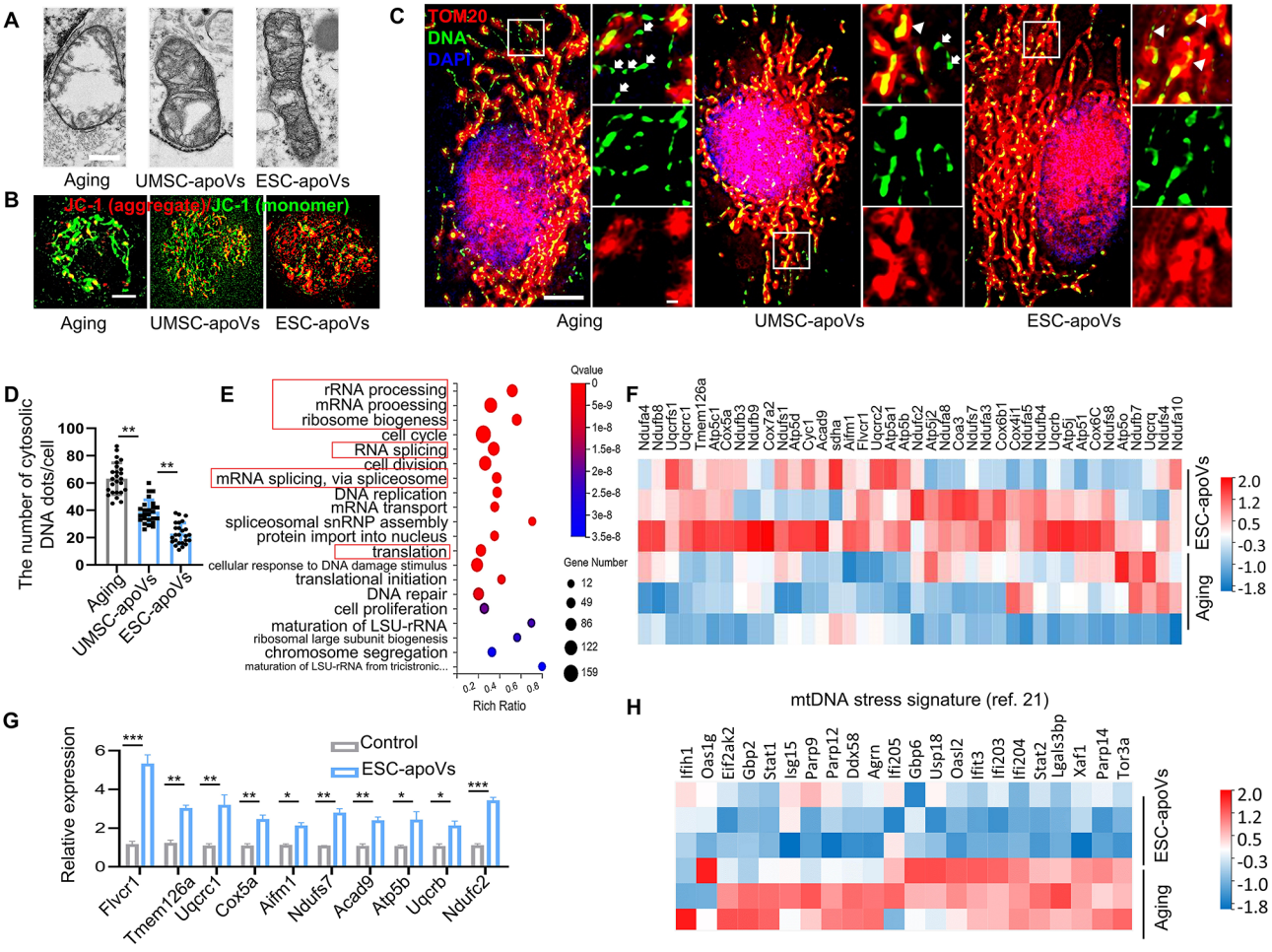

Fig. 4 ESC-apoVs maintains BMMSCs mitochondrial homeostasis by reprogramming mitochondrial transcriptome. **(A)** Representative electron micrographs of the mitochondria from aging BMMSCs cultured with apoVs or PBS. Scale bar, 500 nm ($n = 50$). **(B)** Detection of JC-1 signals in aging BMMSCs by fluorescence confocal microscopy. The double staining of cells by JC-1 is visible either as green for J-monomers or red for J-aggregates. Scale bar, 10 μm ($n = 5$). **C and D.** Representative immunofluorescence images and statistical analysis of TOM20 (red) and DNA (green) in control and apoV-treated aging BMMSCs. Scale bar, 5 μm (left) and 0.5 μm (right) ($n = 25$). **E.** GO enrichment analysis of biological process of upregulated mRNA in ESC-apoVs treated aging BMMSCs. **F.** Heatmap of 40 up-regulated mitochondrial genes in aging BMMSCs treated with ESC-apoVs. **G.** qPCR was performed to determine the relative expression profiles of the top 10 up-regulated genes in aging BMMSCs after treated with ESC-apoVs ($n = 5$). **H.** Heat map revealed that the mtDNA stress signature identified previously [21]. Error bars are mean ± SD. Data were analyzed by one-way ANOVA with Bonferroni test for comparison of multiple groups. $^{*}p < 0.05$, $^{**}p < 0.01$, and $^{***}p < 0.001$

ESC-apoVs inherit TCOF1 to rejuvenate aging BMMSCs

To identify the functional protein present in ESC-apoVs, we analyzed the protein profiles by DIA protein profile analysis [7]. The results showed 3421 differentially expressed genes (DEGs) in ESC-apoVs compared to UMSC-apoVs, consisting of 2425 up-regulated genes and 996 down-regulated genes (Figure S4A). GO enrichment analysis revealed that upregulated proteins in ESC-apoVs were predominantly associated with RNA binding, mRNA binding and translation initiation factor activity, which are closely related to RNA metabolism and transcription (Figure S4B). We used qPCR to verify the top 10 expressed proteins in RNA binding, mRNA binding and translation initiation factor activity domains and found that TCOF1 had the highest expression level (Figure S4C, S4D).

TCOF1 is crucial for the fate of ESCs, and its mutational deficiency can cause Treacher Collins syndrome exhibiting craniofacial malformations [29, 30]. As a transcription factor, TCOF1 is closely related to the transcriptional regulation of multiple proteins, so we further explored whether TCOF1 can repair mitochondrial function in aging BMMSCs by regulating the transcriptional expression of FLVCR1. Western blot analysis revealed that ESC-apoVs contained higher levels of TCOF1 than UMSC-apoVs (Fig. 5A). Additionally, ESC-apoV treatment significantly increased the expression of TCOF1 and FLVCR1 in aging BMMSCs compared to UMSC-apoVs and PBS groups (Fig. 5B). We next used siRNA

Table 1 ESC-apoV treatment upregulated mitochondria-related genes in BMMSCs

Gene ID	Gene Symbol	log2 (ESC-apoV / control)	Pvalue(ESC-apoV / control)
226844	Flvcr1'	1.835009126	1.02E-05
66271	Tmem126a'	1.319689314	8.93E-04
22273	'Uqcrc1'	1.271857687	3.18E-05
12858	'Cox5a'	1.261292404	5.47E-04
26926	'Aifm1'	1.252757677	0.006707846
75406	'Ndufs7'	1.239528287	0.006334547
229211	'Acad9'	1.224747207	0.030802282
11947	'Atp5b'	1.213752443	2.20E-04
67530	'Uqcrb'	1.201678476	0.01943986
68197	'Ndufc2'	1.19689622	0.038596857
66694	'Uqcrfs1'	1.186733193	0.016145095
11946	'Atp5a1'	1.177057889	0.001640591
11949	'Atp5c1'	1.176934928	0.009050318
52469	'Coa3'	1.165191209	0.100599711
227197	'Ndufs1'	1.158907228	0.051334995
66445	'Cyc1'	1.157771846	0.026065994
67003	'Uqcrc2'	1.15184783	0.017431725
12866	'Cox7a2'	1.139927516	0.096253476
110323	'Cox6b1'	1.139706679	0.055494049
68375	'Ndufa8'	1.137780479	0.120204132
11957	'Atp5j'	1.133268818	0.090242994
67264	'Ndufb8'	1.132568882	0.075567611
67273	'Ndufa10'	1.125594109	0.096793043
66495	'Ndufb3'	1.125038055	0.201786057
225887	'Ndufs8'	1.113387248	0.194615139
66945	'Sdha'	1.110099757	0.079253218
12864	'Cox6c'	1.108985726	0.169397879
66043	'Atp5d'	1.104583758	0.100422949
68202	'Ndufa5'	1.097942299	0.344143057
66091	'Ndufa3'	1.094631402	0.255856901
68194	'Ndufb4'	1.091301151	0.311513587
17993	'Ndufs4'	1.079232642	0.426141455
27425	'Atp5l'	1.069076478	0.420072231
17992	'Ndufa4'	1.062731641	0.366110188
12857	'Cox4i1'	1.06184274	0.350651236
28080	'Atp5o'	1.048131022	0.507831236
22272	'Uqcrq'	1.041720096	0.591191268
57423	'Atp5j2'	1.040106052	0.613868541
66218	'Ndufb9'	1.027895597	0.699869859
66916	'Ndufb7'	1.006043813	0.944205525

to knock down TCOF1 expression in ESCs and subsequently generated apoVs. Western blot analysis confirmed that TCOF1 expression was significantly reduced in *siTCOF1*-ESC-apoVs (Fig. 5C). We demonstrated that *siTCOF1*-ESC-apoV treatment failed to upregulate the expression of TCOF1 and FLVCR1 in aging BMMSCs (Fig. 5D). Additionally, *siTCOF1*-ESC-apoV treatment exhibited diminished abilities to restore mitochondrial ultrastructure, specifically mitochondrial swelling and cristae disorder (Fig. 5E). *siTCOF1*-ESC-apoV treatment also failed to rescue the depolarization of mitochondrial membranes in aging BMMSCs and decrease mtDNA leakage (Fig. 5F-I). Furthermore, we used siRNA to knock down FLVCR1 expression in BMMSCs. Western blot analysis confirmed that FLVCR1 expression was significantly reduced in *siFLVCR1*-BMMSCs (Figure S6A). qPCR analysis revealed that ESC-apoV treatment failed to decrease mtDNA release in *siFLVCR1*-BMMSCs (Figure S6C). The data confirm that ESC-apoVs inherit TCOF1 to upregulate FLVCR1, contributing to BMMSC mitochondrial functional homeostasis.

We further verified the effect of *siTCOF1*-ESC-apoVs on the aging phenotype and function of BMMSCs. Immunofluorescence, qPCR and western blot analysis showed that *siTCOF1*-ESC-apoV treatment failed to downregulate the expression of γH2AX, P16, P21, and SA-β-Gal. Additionally, it failed to upregulate the expression of PCNA (Fig. 6A and B, Figure S5A and B). In vitro osteogenic and adipogenic differentiation experiments showed that *siTCOF1*-ESC-apoV treatment failed to rescue the osteogenic and adipogenic differentiation of aging BMMSCs when compared with the control groups (Fig. 6C-F). ELISA analysis revealed that *siTCOF1*-ESC-apoV treatment failed to rescue the levels of SASP-related factors including IL-6, IL-8, MCP-1, and TNF-α (Fig. 6G). Immunofluorescent staining revealed that ESC-apoVs had a diminished ability to rescue senescent levels and proliferation levels in aging *siFLVCR1*-BMMSCs (Figure S6B). These data indicate that ESC-apoVs inherited TCOF1 to rescue the function of aging BMMSCs. Then, we examined whether blocking TCOF1 could abolish the ESC-apoV-induced therapeutic effect in vivo. After 8 weeks of systemic infusion, TCOF1-deficient ESC-apoVs failed to rescue osteogenic ability in vivo, downregulate the expression of γH2AX, P21 and SA-β-Gal, rescue the levels of proliferation and SASP-related factors, and decrease mtDNA leakage (Fig. 7A-D). Collectively, these data suggest that ESC-apoVs inherit TCOF1 to rejuvenate aging BMMSCs and rescue senile osteoporosis *via* FLVCR1-mediated mitochondrial functional homeostasis (Fig. 8).

Discussion

Aging is characterized by the gradual loss of physiological integrity, organs dysfunction, tissue loss of homeostasis and reduced regenerative capacity [31, 32]. Aging is associated with the increased of genomic instability, epigenetic changes, mitochondrial dysfunction, stem cell depletion and cellular senescence, which further accelerate aging [33–35]. Senescent cells, accumulated in aging tissues, exhibit a permanent state of cell cycle arrest, SASP and resistance to apoptosis [22, 26, 33, 36–39]. Apoptosis plays a crucial role in maintaining tissue

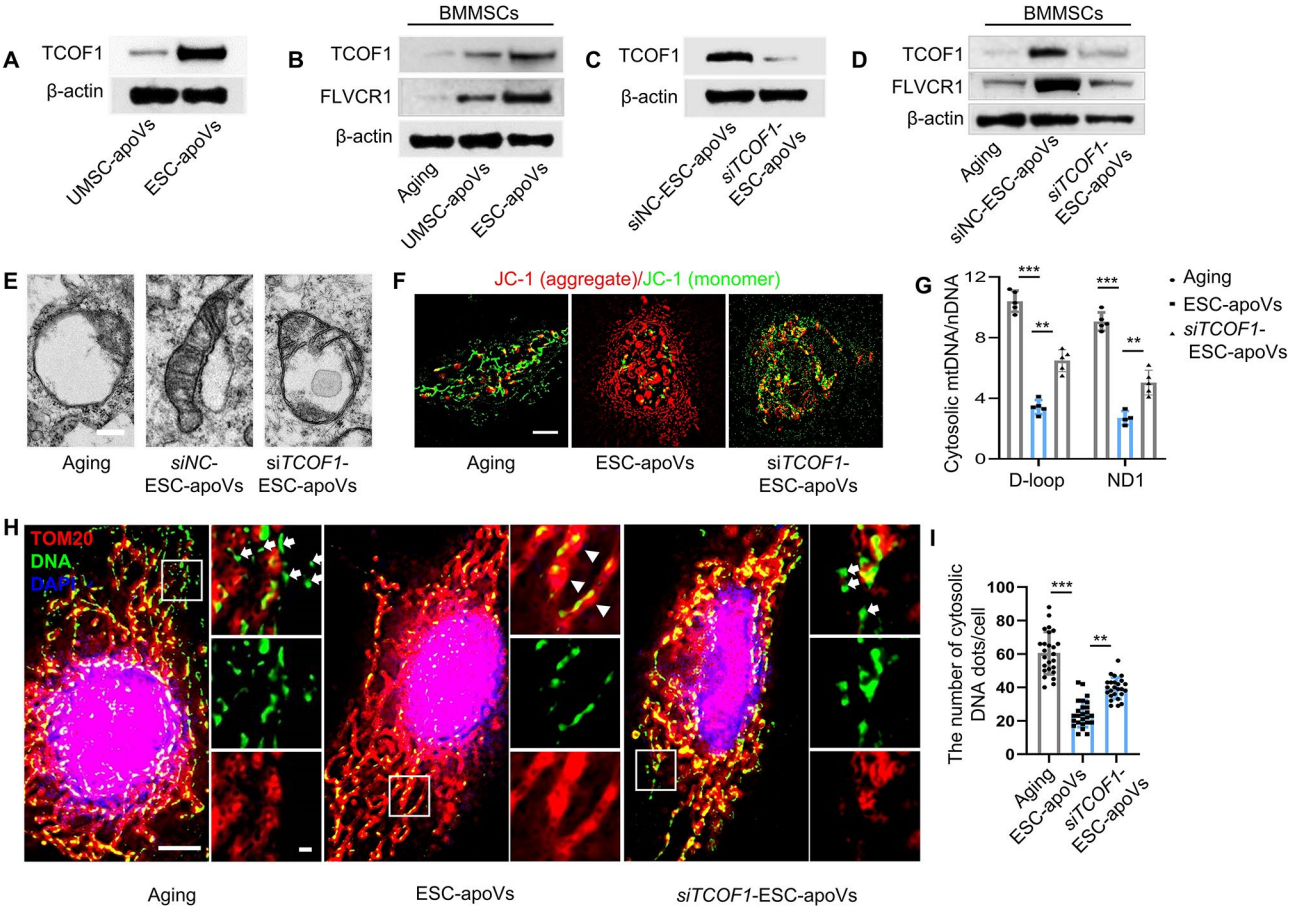

Fig. 5 TCOF1 rescues mitochondrial dysfunction of aging BMMSCs by upregulating mitochondrial protein FLVCR1. **(A)** Western blot analysis showed the expression of TCOF1 in ESC-apoVs and UMSC-apoVs ($n=3$). **(B)** Western blot analysis revealed the expression of TCOF1 and FLVCR1 in aging BMMSCs cocultured with apoVs or PBS ($n=3$). **(C)** Western blot analysis showed the expression of TCOF1 in *siNC*-ESC-apoVs and *siTCOF1*-ESC-apoVs ($n=3$). **(D)** Western blot analysis revealed the expression of TCOF1 and FLVCR1 in aging BMMSCs cocultured with *siNC*-ESC-apoVs and *siTCOF1*-ESC-apoVs ($n=3$). **(E)** Representative electron microscope images of mitochondria from aging BMMSCs cultured with *siNC*-ESC-apoVs, *siTCOF1*-ESC-apoVs or PBS. Scale bar, 500 nm ($n=50$). **(F)** Detection of JC-1 signals in aging BMMSCs by fluorescence confocal microscopy. The double staining of cells by JC-1 is visible either as green for J-monomers or red for J-aggregates. Scale bar, 10 μm ($n=5$). **(G)** qPCR analysis of mtDNA release in aging BMMSCs ($n=5$). **H and I.** Representative immunofluorescent images and statistical analysis of TOM20 (red) and DNA (green) in control and aging BMMSCs treated with *siNC*-ESC-apoVs or *siTCOF1*-ESC-apoVs. Scale bar, 5 μm (left) and 0.5 μm (right) ($n=25$). Error bars are mean ± SD. Data were analyzed by one-way ANOVA with Bonferroni test for comparison of multiple groups. $^{**}p<0.01$, and $^{***}p<0.001$

homeostasis and eliminating potentially harmful cells [4, 40]. The increased age-related resistance to apoptosis could accelerate the aging process [36]. Current research suggests that bone aging is accompanied by an increase in osteoblast apoptosis and a decrease in osteoclast apoptosis [41]. However, lack of studies on the overall apoptosis alteration in bone tissue and its impact on bone aging. Current anti-aging research mainly focuses on senolytics to treat senescent osteoporosis by targeting anti-apoptotic pathways to increase the level of apoptosis of senescent cells [42, 43]. However, it is still elusive whether apoptotic metabolites can alleviate aging. In this study, we demonstrated that apoptosis resistance in aging mice compromised their osteogenic capacity. Systemic infusion of exogenous ESC-apoVs dramatically rescued impaired BMMSCs and SOP via reusing ESC-apoV-derived TCOF1 to maintain mitochondrial homeostasis.

Billions of cells undergo apoptosis every day in the human body to generate significant amounts of apoVs [44]. ApoVs, a specific type of EVs, contain a variety of DNAs, RNAs, proteins, lipids, and nuclear components [45–48]. We identified that apoVs express specific markers such as cleaved caspase 3, calnexin, and calreticulin when compared with exosomes [6, 7, 48]. In addition, our previous study firstly demonstrated that apoVs are required to maintain mesenchymal stem cell homeostasis and rescue the osteoporosis phenotype by transferring miRNA [5]. ApoVs are capable of promoting wound healing and hair regeneration via activation of Wnt/b-catenin pathway in skin and hair follicle MSCs [9]. Embryonic stem cells are pluripotent stem cells that can self-renew

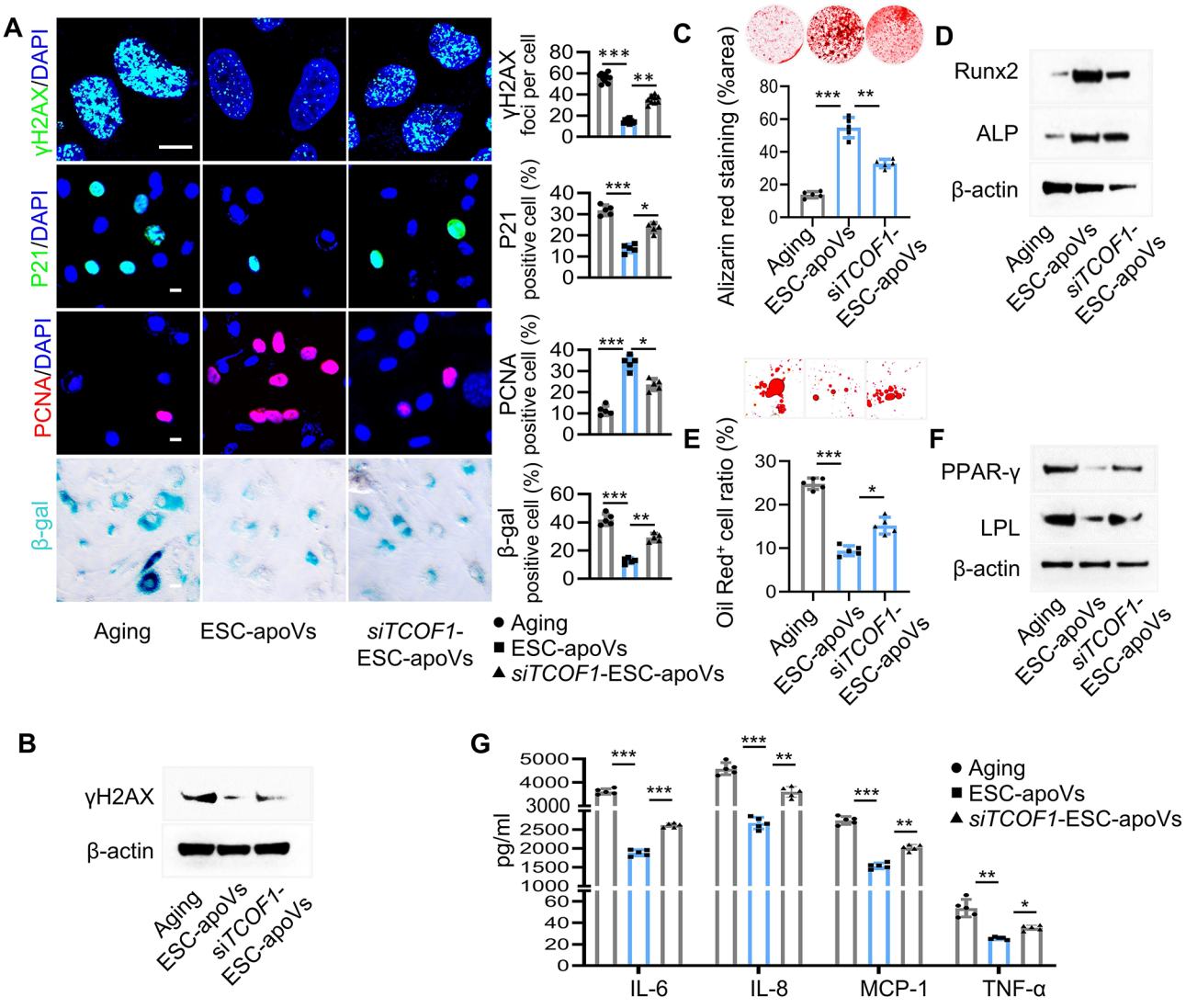

Fig. 6 TCOF1 ameliorates impaired BMMSCs and age-related hallmarks. **(A)** Immunofluorescent images and semi-quantification of γH2AX foci ($n=10$), P21, PCNA and β-Gal ($n=5$) in *siTCOF1*-ESC-apoV-treated BMMSCs. Scale bar, 10 μm. **(B)** Western blot showed expression of senescence marker γH2AX in aging BMMSCs cocultured with *siTCOF1*-ESC-apoVs ($n=3$). **C and D.** Osteogenesis of aging BMMSCs cocultured with *siTCOF1*-ESC-apoVs as assessed by Alizarin red staining ($n=5$) and Western blot ($n=3$). **E and F.** Adipogenesis of aging BMMSCs cocultured with *siTCOF1*-ESC-apoVs as assessed by Oil Red O staining ($n=5$) and Western blot ($n=3$). **G.** The expression of SASPs factors in aging BMMSCs cocultured with *siTCOF1*-ESC-apoVs ($n=5$). Error bars are mean ± SD. Data were analyzed by one-way ANOVA with Bonferroni test for comparison of multiple groups. *$p<0.05$, **$p<0.01$, and ***$p<0.001$

indefinitely and differentiate into any tissue cell in the body [49, 50], providing them potential for regenerative applications [11, 51]. Our previous study demonstrated that apoVs derived from ESCs play a significant role in maintaining the stemness of MSCs via activation of hippo pathway [7]. Here, we demonstrate that ESC-apoVs inherit TCOF1 from their parent cells to rejuvenate aging BMMSCs and ameliorate senile osteoporosis.

Culture-expanded MSCs typically express low levels of MHC class I and do not express MHC class II or co-stimulatory molecules (such as B7-1, B7-2, or CD40) [22, 52, 53], making MSCs and ESCs low immunogenic or "immune privileged". This property is thought to enable MSCs and ESCs transplantation across major histocompatibility barriers. Apoptotic vesicles have the immunogenic MHC molecules similar to their parental cells, there is not report to show apoVs cause any immune rejection response.

Mitochondrial dysfunction, as well as its morphology, has been associated with aging and many aging-associated pathological conditions, including cancer, neurodegenerative diseases, metabolic diseases and others [15, 54]. Mitochondrial dysfunction has also been found in stress-induced senescence [55, 56], replicative senescence [57], oncogene-induced senescence [58], and senescence triggered by genetic telomere uncapping [56].

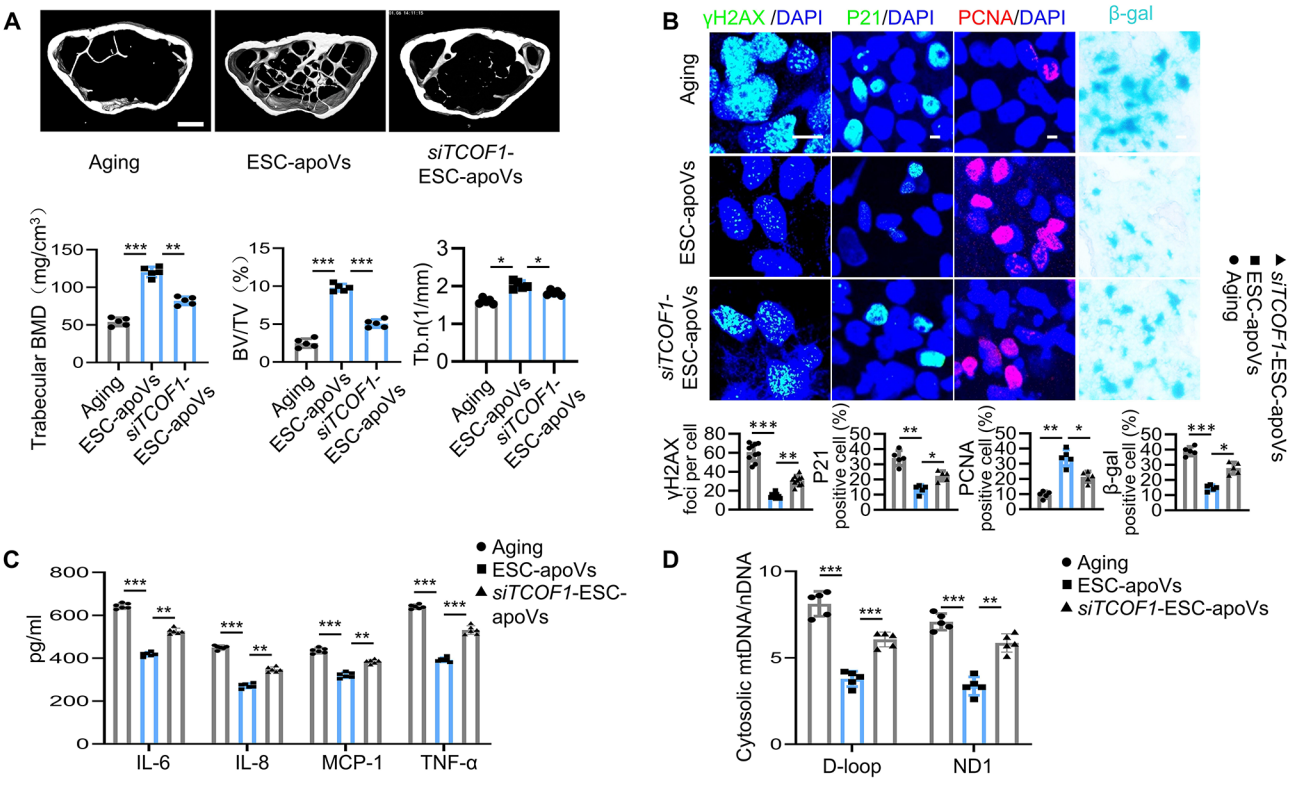

Fig. 7 ESC-apoVs contained TCOF1 ameliorate bone phenotypes in aging mice. **A**. MicroCT images and analysis of the distal femurs in aging mice with *siTCOF1*-ESC-apoV treatment ($n=5$). Scale bar, 0.5 mm. **B**. Immunofluorescent images and quantification of γH2AX foci ($n=10$), P21, PCNA and β-Gal ($n=5$) in mouse bone marrow after *siTCOF1*-ESC-apoV treatment. Scale bar, 10 μm. **(C)** Expression of SASPs in the serum of mice with *siTCOF1*-ESC-apoV treatment ($n=5$). **(D)** Quantification of cmtDNA and total mtDNA in bone marrow of aging mice with *siTCOF1*-ESC-apoV treatment ($n=5$). Error bars are mean ± SD. Data were analyzed by one-way ANOVA with Bonferroni test for comparison of multiple groups. *$p<0.05$, **$p<0.01$, and ***$p<0.001$

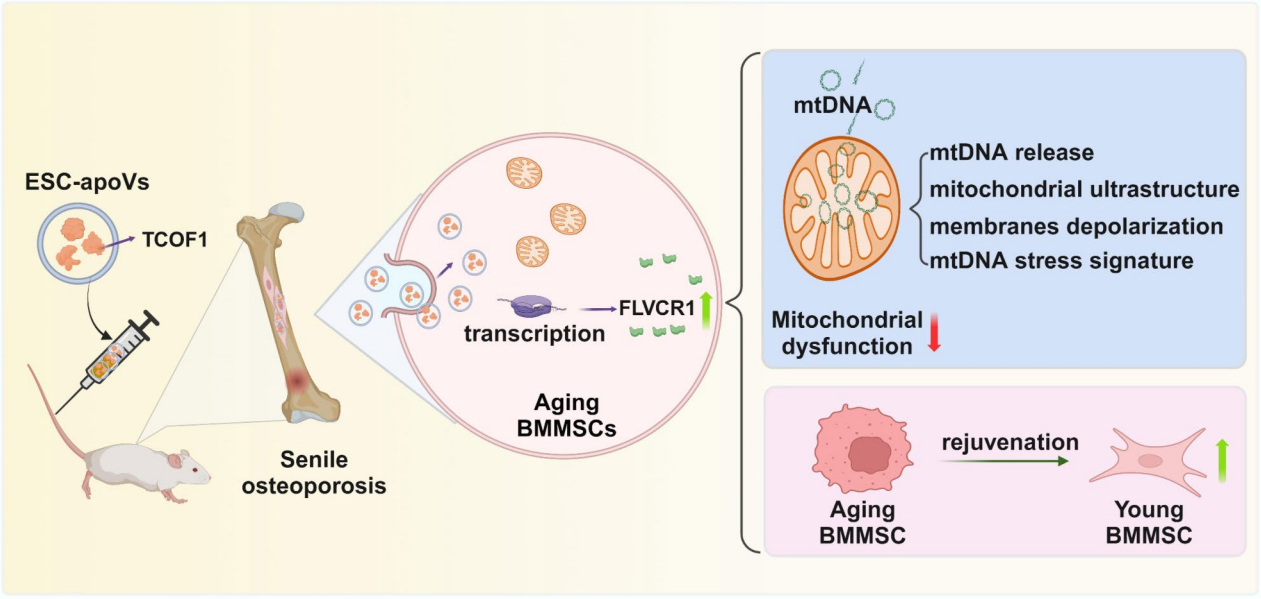

Fig. 8 Schematic drawing of ESC-apoVs inheriting TCOF1 to maintain mitochondrial homeostasis in aging BMMSCs *via* upregulation of FLVCR1

Importantly, specific ablation of impaired mitochondria from senescent cells was sufficient to reverse many features of the senescent phenotype [59]. Therefore, therapies targeting mitochondrial dysfunction in senescent cells are expected to offer new treatment options for improving aging. Recent studies have found that the release of mitochondrial DNA (mtDNA) into the cytoplasm activates the cGAS–STING pathway and accelerates the aging process [19–21, 60]. It is suggested that reducing mtDNA leakage may be an effective strategy to alleviate aging. In this study, we found that increased levels of apoptosis and apoptotic metabolites significantly attenuate mtDNA release and reduce aging hallmarks of aging mice.

TCOF1 is a nucleolar factor that regulates transcription in nucleolus through interacting with the upstream binding factor (UBF) [29]. TCOF1 was initially discovered as a gene involved in Treacher Collins syndrome, a rare genetic disorder characterized by severe craniofacial deformations [61]. From the molecular perspective, TCOF1 is necessary for proper rDNA transcription [62], as well as biogenesis and modifications of ribosomes, contributing to the translation patterns in the cell [30]. At the cellular level, TCOF1 contributes to the regulation of mitosis and proliferation [63, 64]. In this study, we found that TCOF1 can promote the transcription of mitochondrial functional proteins and restore mitochondrial dysfunction in aging cells. Feline leukemia virus subgroup C receptor (FLVCR1) is a cell surface heme exporter, essential for erythropoiesis and systemic iron homeostasis [65]. Recently, study showed that *FLVCR1* depletion leads to changes in mitochondrial membrane structure [28]. This study found that TCOF1 significantly increased the expression level of FLVCR1 in mitochondria, leading to the restoration of mitochondrial function.

This study reveals a previously unknown role of apoptosis and apoptotic metabolites in maintain bone homeostasis of aging. In addition, ESC-apoVs inherit TCOF1 from their parent cells to ameliorate senile osteoporosis *via* FLVCR1-mediated mitochondrial homeostasis, offering a newly effective approach for the therapy of age-related diseases.

Materials and methods

Animals

6-week-old and 15-month-old C57BL/6J mice were purchased from Model Animal Research Center of Nanjing University and Gempharmatech Company, Nanjing, China. Cdkn2a-Luc-2 A-tdTomato-2 A-CreERT2 mice (NM-KI-18039) were purchased from Shanghai Model Organisms Center. All animal experiments were conducted in accordance with the guidelines of the Institutional Animal Care and Use Committee under an approved protocol at Sun Yat-Sen University (SYSU-IACUC-2023-B1163).

Antibodies and reagents

All antibodies, cytokines, kit, and other recourse used in this study are listed in Table 2.

Cell culture and induction of senescent cells

Human ESCs were generously provided by the research group of Junjun Ding at Sun Yat-sen School of Medicine. Human umbilical cord mesenchymal stem cells (UMSCs) and mouse bone marrow MSCs (mBMMSCs) were isolated and cultured as described in our previous studies [5, 48]. Briefly, UMSCs were obtained from full-term cesarean section surgery with the informed consent of the donors and cultured in MEM alpha basic medium (α-MEM, Invitrogen) with 15% fetal bovine serum (FBS, Gibco), L-ascorbic acid phosphate ($0.1\times10-3$ M, Wako), and 1% penicillin/streptomycin (Invitrogen).

mBMMSCs were isolated from the bone marrow of femurs and tibias of C57BL/6J mice. And then mBMMSCs were cultured in alpha minimum essential medium (α-MEM, Invitrogen) with 20% FBS (Gibco), 2 mM L-glutamine (Invitrogen), 55 mM 2-mercaptoethanol (Invitrogen), and 1% penicillin/streptomycin (Invitrogen). mBMMSCs were seeded into 24-well plates (3×10^4 cells/well) and cocultured with 3.75×10^7 apoVs derived from ESCs or UMSCs for 24 h. All cells utilized in this study and relevant experiments were approved by the Medical Ethics Committee of the Hospital of Stomatology, Sun Yat-Sen University (KQEC-2021-59-01).

Apoptosis modulation

For in vivo analysis of apoptotic rate, STS (120 ng/kg body weight) was administered intraperitoneally (i.p.). Administered to mice twice a week for 8 weeks, as previously reported. STS was used to induce apoptosis in ESCs and UMSCs. ESCs and UMSCs were treated with 500 nM STS for 8 h at 37 °C.

Isolation of ApoVs

ApoVs were isolated using the method of differential centrifugation as previously described [48]. When the cultured cells reach 85% density, cells were washed twice with 0.1 μm-filtered PBS and the medium was substituted with α-MEM and 250 nM staurosporine (STS, Enzo Life Sciences, USA). After 8 h treatment, apoVs were isolated from the medium of apoptotic MSCs using sequential centrifugation followed by sequential filtering. Briefly, the supernatant containing apoVs were harvested and centrifuged at 800 g for 10 min, followed by centrifugation at 2000 g for another 10 min to remove cell debris. Subsequently, the supernatant containing apoVs was centrifuged at 16,000 g for 30 min to collect apoVs pellets.

Table 2 Reagents

Reagent or Antibodies	Source	Identifier
Anti-Phospho-Histone H2A.X-Rabbit	CST	9718S
Anti-Cleaved Caspase-3 -Rabbit	CST	9664s
Anti-TSG101-Rabbit	Abcam	ab125011
Anti-P21-rabbit	Abcam	ab188224
Anti-Tom20-mouse	Abcam	ab283317
Anti-DNA-mouse	Millipore Sigma	CBL186
Anti-β-actin-mouse	Sigma	A5441
Anti-TCOF1- Rabbit	Abcam	Affinity Biosciences
Anti-FLVCR1- Rabbit	Proteintech Group	26841-1-AP
Anti-Runx2- Rabbit	Abcam	ab236639
Anti-ALP- Rabbit	invitrogen	PA5106391
Anti-PPAR-γ-mouse	Santa Cruz	sc-7273
Anti-LPL- Rabbit	invitrogen	PA571881
FITC Annexin V	Biolegend	640906
Alexa Fluor™ 568 goat anti-rabbit IgG(H + L)	Invitrogen	A11036
Alexa Fluor™ 488 goat anti-rabbit IgG(H + L)	Invitrogen	A11008
Alexa Fluor™ 568 goat anti-mouse IgG(H + L)	Invitrogen	A11004
Alexa Fluor™ 488 goat anti-mouse IgG(H + L)	Invitrogen	A11001
β-Galactosidase Staining Kit	Solarbio	G1580-100T
PKH26 Red Fluorescent Cell Linker kit	Sigma-Aldrich	PKH26GL-1KT
Staurosporine	Enzo Life Sciences	ALX-380-014
Mounting Medium with DAPI	Abcam	ab104139
RIPA Lysis Buffer System	Santa Cruz	sc-24948
Dexamethasone	Sigma-Aldrich	D4902
Staurosporine	Enzo Life Sciences	ALX-380-014
TritonTM X-100	Sigma-Aldrich	X100-100ML
α-MEM	Invitrogen	12571-048
Fetal bovine serum (FBS)	Gibco	10270-106
L -glutamine	Invitrogen	35050-061
2-mercaptoethanol	Invitrogen	21985-023
Penicillin-Streptomycin	Invitrogen	15140-122
TrypLETM Express Enzyme	Invitrogen	12605-010
10X Annexin V Binding Buffer	BD Pharmingen	556454
NuPAGE MES SDS Running Buffer	Invitrogen	NP0002
NuPAGE Transfer Buffer	Invitrogen	NP00061
PageRuler™ Prestained Protein Ladder	Invitrogen	26616
Novex™ Sharp Pre-stained Protein Standard	Invitrogen	LC5800
NuPAGE™ LDS Sample Buffer	Invitrogen	NP0007
Lipofectamine™ RNAiMAX Transfection Reagent	Invitrogen	13778
Opti-MEM Medium	Invitrogen	31985070

The pallets were then resuspended in PBS and diluted with ultrapure water.

Nanoparticle tracking analysis (NTA)

For size distribution evaluation, nanoparticle tracking analysis (NTA) was performed by using ZetaView® PMX120 (Particle Metrix, Germany). ApoVs were diluted in 0.1 μm-filtered PBS. The particle size distribution and potential were measured. Measurements were done at all 11 positions and the video quality was set to medium. Data were analyzed using the ZetaView® analysis software (Version 8.02.31) with a minimum size of 10, a maximum size of 5000, and a minimum brightness of 30.

Nano flow cytometry (nFCM)

Nano flow cytometry (NanoFCM, Xiamen, China) was used to analyze surface molecules of apoVs. Newly isolated apoVs were treated with cleaved caspase 3 antibodies for immunofluorescence analysis. nFCM equipped with single photon counting avalanche photodiodes was used for the simultaneous detection of side scatter (SSC) and fluorescence of individually stained apoVs. Before analyzing apoVs samples, the nFCM was calibrated for particle concentration with 200 nm AF488 fluorophore conjugated polystyrene beads, and then Silica Nanosphere Cocktail (NanoFCM Inc., S16M-Exo) was used to create a standard curve as a reference. After setting up acquisition parameters including laser power, detection threshold and detector gain, stained apoVs were injected into the nFCM and collected within 1 min to calculate the total number of particles and number of positive particles using NanoFCM software (NanoFCM Professional Suite V1.15).

TUNEL assay

Frozen sections were fixed with 4% PFA and permeabilized. Samples were incubated with the TUNEL reaction mix (#G3250, Promega) for 60 min at 37 °C. After counterstaining with DAPI, TUNEL-positive cells were counted using an inverted optical microscope with a magnification of 200× (Zeiss, Germany).

Immunofluorescence staining

Frozen sections and cell samples were fixed in 4% paraformaldehyde (Sigma-Aldrich) for 20 min at room temperature. Subsequently, the samples were stained with primary antibodies, followed by secondary antibody staining. Finally, the samples were sealed with a DAPI sealing agent and mounted on adhesive microscope slides.

Western blotting

Total protein was extracted using a protein extraction kit (Thermo, Rockford, IL, USA) according to the

manufacturer's instructions. 20 μg protein of each sample was loaded onto SDS-polyacrylamide electrophoresis gels and transferred to PVDF membranes (Millipore). Subsequently, the membranes were blocked for 1 h, then incubated with primary antibodies at 4 °C overnight, followed by incubation with the HRP-conjugated secondary antibodies for 1 h at room temperature. Finally, immunoreactive proteins were visualized using SuperSignal West Pico Chemiluminescent Substrate (Thermo Fisher) and detected with a gel.

ELISA

According to the manufacturer's protocol, the levels of human IL-6, IL-8, TNF-α and MCP-1 concentration were measured using human ELISA Quantikine Immunoassay kit (CUSABIO, China), and the levels of mouse IL-6, IL-8, TNF-α and MCP-1concentration were measured using human ELISA Quantikine Immunoassay kit (Maisha, China).

TEM

Cells were postfixed in 2.5% glutaraldehyde for 4 h at 4 °C (Wuhan Goodbio Technology Co., Ltd, China), then fixed in 1% osmium tetroxide (OsO4; Sinopharm Chemical Reagents Co., Ltd., China) in 0.1 M PBS for 1 h at room temperature. Following dehydration with ethanol (Sinopharm Chemical Reagent Co., Ltd., China), the cells were embedded in Epon resin (Sales Performance International Greater China Co., China), and ultrathin sections of the selected areas were cut using an LKB NOVA ultramicrotome (Leica Biosystems, Germany) with a diamond knife (Daito Me Holdings Co., Ltd, Japan). Cells were then stained with a saturated solution of uranyl acetate in methanol (50:50) (Sinopharm Chemical Reagent Co., Ltd., China) for 12 min at 45 °C, followed by incubation in an aqueous solution of concentrated bismuth subnitrate (Sinopharm Chemical Reagent Co., Ltd., China) for 10 min at 25 °C. Subsequently, all the sections were examined under a Hitachi TEM system (Hitachi, Ltd., Japan).

SA-β-galactosidase staining

The cellular senescence of frozen sections and MSCs was assessed according to the manufacturer's protocol for β-galactosidase Staining Kit (Solarbio). The percentage of senescent cells was evaluated by the ratio of positive cells to the total number of cells obtained from five different fields of view. The experiments were repeated at least three times.

Mitochondrial membrane potentials assay

JC-1 probe was employed to evaluate the mitochondrial depolarization in mBMSCs. Briefly, cells incubated with an equal volume of serum-free medium containing JC-1 dye (5 mg/L) at 37 °C for 20 min and rinsed twice with PBS, then placed in fresh medium without serum. Finally, images were taken in the green and red fluorescence channel. The images were obtained at 488 nm excitation and 530 nm emission for green (JC-1 monomers) and at 543 nm excitation and 590 nm emission for red fluorescence (JC-1 aggregates).

Micro CT and analysis

22-month-old mice were used for the experiments. We intravenously infused 1.6×10^{10} of ESC-apoVs, UMSC-apoVs or PBS per mouse twice a week for two consecutive months as reported previously [7]. Mice were sacrificed at 24 months of age. Femurs were fixed in 4% paraformaldehyde and analyzed using a Venus Micro CT (PINGSENG Healthcare, China) with the scan parameters of tube voltage 90 KV, tube current 70 μA, and voxel size 13 μm. Data were visualized and analyzed using Avatar software (PINGSENG Healthcare, China).

Bioluminescence Imaging

Heterozygous Cdkn2a-Luc-2 A-tdTomato-2 A-CreERT2 mice can be stimulated to bioluminescence by injection of luciferase substrate as reported previously [66]. Cdkn2a-Luc-2 A-tdTomato-2 A-CreERT2 mice were injected intraperitoneally with 3 mg d-luciferin in 200 μl PBS. Mice were anesthetized using isoflurane and bioluminescence images were acquired using a Xenogen IVIS 100 (PerkinElmer, USA) according to the manufacturer's instructions. The fluorescence intensity was quantified with Living Image software (PerkinElmer, USA).

qPCR analysis of cytosolic DNA

The experiment was performed as previous described [67]. Briefly, 20,000 mBMMSCs cells were collected and resuspended in 250mL NaCl-HEPES buffer (150 mM NaCl, 20 mM HEPES pH 7.4, 25 mg/mL digitonin). After incubated on ice for 5 min, the homogenates were incubated end over end for 23 min to allow selective plasma membrane permeabilization, then centrifuged at 1,000 g for 5 min at 4℃. The pellets were resuspended in 500 mL of 50 mMNaOH and boiled for 30 min at 98℃ to solubilize DNA, and then add 100 mL 1 M Tris-HCl pH 8.0 to neutralize the pH, and these extracts served as normalization controls for total nDNA. The cytosolic supernatants were transferred to fresh tubes and spun at 17,000 g for 10 min at 4℃ to remove any remaining cellular debris, and used directly for cytosolic mtDNA quantification (1 mL). Quantitative PCR was performed on both whole-cell extracts and cytosolic fractions using nuclear DNA primers (Tert) and mtDNA primers (D loop and ND1), and the CT values obtained for nDNA abundance for whole-cell extracts served as normalization controls for the mtDNA values obtained from the cytosolic

fractions. The oligonucleotides for qPCR analysis were listed in Table 3.

DIA analysis

Proteins were analyzed using Q-Exactive HF X (Thermo Fisher Scientific, San Jose, CA). Proteins were extracted with 1 x cocktail with the appropriate amounts of SDS L3 and EDTA, followed by centrifuging for 15 min at 25,000×*g* at 4 °C. The supernatants were collected to undergo Bradford quantification and SDS-PAGE analysis. The proteins were also enzymatically hydrolyzed using Trypsin enzyme and separated with High pH RP to obtain freeze-dried peptide samples. For data-dependent acquisition (DDA) analysis, LC-separated peptides were ionized by nanoESI and injected into a Q-Exactive HF X tandem mass spectrometer (Thermo Fisher Scientific, San Jose, CA) in DDA detection mode. For data-independent acquisition (DIA) analysis, LC-separated peptides were ionized by nanoESI and injected into a Q-Exactive HF X (Thermo Fisher Scientific, San Jose, CA) tandem mass spectrometer in DIA detection mode. Based on the sample data generated from a high-resolution mass spectrometer, DDA data was identified by Andromeda search engine within MaxQuant version 1.5.3.30, and identification results were used for spectral library construction. For large-scale DIA data, mProphet algorithm was used to perform quality control. For MSstats differential analysis, differential protein screening was performed based on fold change > 1.5 and $P < 0.05$ as the criteria for significance. Identified proteins were annotated and classified into pathways using Gene Ontology (GO) and the Kyoto Encyclopedia of Genes and Genomes (KEGG) database, respectively. Based on the quantitative results, the differential proteins between comparison groups were identified for functional enrichment and subcellular localization analysis.

RNA sequencing (RNA-seq) analysis

RNA samples were isolated using TRIzol reagent (Invitrogen, USA) and quantified, followed by cDNA library construction and sequencing performed by Beijing Genomics Institute (BGI) using BGISEQ-500 platform. Bioinformatics workflow including data filtering, mapping transcript prediction, differential gene expression analysis as well as GO and Pathway analysis were performed following procedures established at BGI. An average of about 6.16G Gb bases per sample were generated with an average mapping ratio of 95.20%.

Table 3 Oligonucleotides

mtDNA/nDNA primers	
m-nDNA-Tert -qPCR-F	CTAGCTCATGTGTCAAGACCCTCTT
m-nDNA-Tert -qPCR-R	GCCAGCACGTTTCTCTCGTT
mD-loop-qPCR1-F	AATCTACCATCCTCCGTGAAACC
mD-loop-qPCR1-R	TCAGTTTAGCTACCCCCAAGTTTAA
mD-loop-qPCR3-F	TCCTCCGTGAAACCAACAA
mD-loop-qPCR3-R	AGCGAGAAGAGGGGCATT
mND1-M-qPCR-F	CTAGCAGAAACAAACCGGGC
mND1-M-qPCR-R	CCGGCTGCGTATTCTACGTT
mGAPDH-qPCR-F	GACTTCAACAGCAACTCCCAC
mGAPDH-qPCR-R	TCCACCACCCTGTTGCTGTA

siRNA transfection

For siRNA transfection, ESCs were transfected with TCOF1 siRNA (Ribo, China), mBMMSCs were transfected with FLVCR1 siRNA (Ribo, China) using Lipofectamine RNAiMAX transfection reagent (Thermo Fisher, USA) according to the manufacturer's instructions. Nontargeting control siRNAs (Ribo, China) were used as negative controls. Transfection efficiency was evaluated by Western blotting.

Osteogenic differentiation assay

mBMMSCs were seeded on 6-well plate. The medium was replaced with osteogenic medium containing 2 mM β-glycerophosphate (Sigma), 100 μM Lascorbicacid 2-phosphate (Sigma) and 10 nM dexamethasone (Sigma) when cells reached 100% confluence. After four weeks of osteogenic induction, the cultures were stained with 1% alizarin red-S (Sigma). Alizarin red-positive area was analyzed using Image J software (NIH) and shown as a percentage of the total area.

Adipogenic differentiation

mBMMSCs were seeded on 6-well plate. The medium was replaced with adipogenic medium containing 500nM isobutylmethylxanthine (Sigma-Aldrich), 60μM indomethacin (Sigma-Aldrich), 500nM hydrocortisone (Sigma-Aldrich), 10 μg/ mL insulin (Sigma-Aldrich), and 100nM L-ascorbic acid phosphate when cells reached 100% confluence. At four weeks post-induction, the adipocytes were stained with Oil red O (Sigma-Aldrich), and positive cells were quantified under microscopy and shown as a number out of the total number of cells.

TRAP/ALP staining

Frozen sections were stained with TRAP/ALP Stain Kit (Wako Pure Chemical Industries Ltd., Osaka, Japan) in accordance with the manufacturer's instructions. Red-stained multinucleated (TRAP-positive) cells were defined as osteoclasts. The images were examined under an optical microscope (Zeiss, Germany).

Statistical analysis

All experiments were performed in biological triplicate and data were expressed as mean ± standard deviation (SD). Statistical and graph analysis were performed by GraphPad Prism 7 (GraphPad Software, USA). Multiple

group comparisons were assessed by one-way ANOVA analysis with Tukey's test. For two-group comparisons, significance was analyzed using independent unpaired two-tailed Student's t tests. Values of $P<0.05$ were considered as statistically significant.

Supplementary Information

The online version contains supplementary material available at https://doi.org/10.1186/s12951-024-02820-x.

Supplementary Material 1

Acknowledgements

This work was supported by grants from the National Natural Science Foundation of China (82301123 to Y.Q., 82401162 to B.M.), the Natural Science Foundation of Guangdong Province (2023A1515010626, 2024A1515012820 to Y.Q., 2023A1515111127 to B.M.), China Postdoctoral Science Foundation (2024M753797 to Y.Q, 2024M753795 to B.M.), the Guangzhou Basic and Applied Basic Research Scheme (SL2024A04J02205 to Y.Q.), and the nationally Funded Postdoctoral Researcher Program (GZC20233267 to B.M.), the National Key R&D Program of China (2021YFA1100600 to S.S.), the Pearl River Talent Recruitment Program (2019ZT08Y485, 2019QN01Y138, 2019JC01Y182), the Guangdong Financial Fund for High-Caliber Hospital Construction (174-2018-XMZC-0001-03-0125, D-07 to S.S.).

Author contributions

Y.Q. contributed to designing study plan, performing experimental procedures and drafting manuscript. B.M. contributed to designing study plan, data acquisition and drafting manuscript. B.Y. and C.F. contributed to data analysis and interpretation. Y.H. contributed to data analysis and illustrating all the schematic diagrams. X.L. contributed to the analysis of mouse bone marrow. P.L. contributed to protein extraction. Z.C. contributed to the analysis of protein profile. S.S. and W.T. contributed to the project conception, experimental design, writing manuscript and supervision. All authors approved the final version of the manuscript.

Data availability

No datasets were generated or analysed during the current study.

Declarations

Ethics approval and consent to participate

All animal experiments were conducted in accordance with the guidelines of the Institutional Animal Care and Use Committee under an ethical review approval at Sun Yat-Sen University (SYSU-IACUC-2023-B1163).

Competing interests

The authors declare no competing interests.

Received: 31 May 2024 / Accepted: 30 August 2024
Published online: 06 September 2024

References

1. Medina CB, Mehrotra P, Arandjelovic S, Perry JSA, Guo Y, Morioka S, Barron B, Walk SF, Ghesquière B, Krupnick AS, Lorenz U, Ravichandran KS. Metabolites released from apoptotic cells act as tissue messengers. Nature. 2020;580(7801):130–5.
2. Fuchs Y, Steller H. Programmed cell death in animal development and disease. Cell. 2011;147(4):742–58.
3. Singh B, Maiti GP, Zhou X, Fazel-Najafabadi M, Bae SC, Sun C, Terao C, Okada Y, Heng Chua K, Kochi Y, Guthridge JM, Zhang H, Weirauch M, James JA, Harley JB, Varshney GK, Looger LL, Nath SK. Lupus Susceptibility Region containing CDKN1B rs34330 mechanistically influences expression and function of multiple target genes, also linked to proliferation and apoptosis. Arthritis Rheumatol (Hoboken N J). 2021;73(12):2303–13.
4. Tang D, Kang R, Berghe TV, Vandenabeele P, Kroemer G. The molecular machinery of regulated cell death. Cell Res. 2019;29(5):347–64.
5. Liu D, Kou X, Chen C, Liu S, Liu Y, Yu W, Yu T, Yang R, Wang R, Zhou Y, Shi S. Circulating apoptotic bodies maintain mesenchymal stem cell homeostasis and ameliorate osteopenia via transferring multiple cellular factors. Cell Res. 2018;28(9):918–33.
6. Zheng C, Sui B, Zhang X, Hu J, Chen J, Liu J, Wu D, Ye Q, Xiang L, Qiu X, Liu S, Deng Z, Zhou J, Liu S, Shi S, Jin Y. Apoptotic vesicles restore liver macrophage homeostasis to counteract type 2 diabetes. J Extracell Vesicles 2021, 10 (7), e12109.
7. Qu Y, He Y, Meng B, Zhang X, Ding J, Kou X, Teng W, Shi S. Apoptotic vesicles inherit SOX2 from pluripotent stem cells to accelerate wound healing by energizing mesenchymal stem cells. Acta Biomater. 2022;149:258–72.
8. Wang J, Cao Z, Wang P, Zhang X, Tang J, He Y, Huang Z, Mao X, Shi S, Kou X. Apoptotic extracellular vesicles ameliorate multiple myeloma by restoring Fas-mediated apoptosis. ACS Nano. 2021;15(9):14360–72.
9. Ma L, Chen C, Liu D, Huang Z, Li J, Liu H, Kin Kwok RT, Tang B, Sui B, Zhang X, Tang J, Mao X, Huang W, Shi S, Kou X. Apoptotic extracellular vesicles are metabolized regulators nurturing the skin and hair. Bioact Mater. 2023;19:626–41.
10. Huang Z, Zhuang Y, Li W, Ma M, Lei F, Qu Y, Li J, Luo H, Li C, Lu L, Ma L, Zhang X, Kou X, Jiang L, Mao X, Shi S. Apoptotic vesicles are required to repair DNA damage and suppress premature cellular senescence. J Extracell Vesicles 2024, 13 (4), e12428.
11. Yamanaka S. Pluripotent stem cell-based Cell Therapy-Promise and challenges. Cell Stem Cell. 2020;27(4):523–31.
12. Damdimopoulou P, Rodin S, Stenfelt S, Antonsson L, Tryggvason K, Hovatta O. Human embryonic stem cells. Best Pract Res Clin Obstet Gynecol. 2016;31:2–12.
13. Shpilka T, Haynes CM. The mitochondrial UPR: mechanisms, physiological functions and implications in ageing. Nat Rev Mol Cell Biol. 2018;19(2):109–20.
14. Amorim JA, Coppotelli G, Rolo AP, Palmeira CM, Ross JM, Sinclair DA. Mitochondrial and metabolic dysfunction in ageing and age-related diseases. Nat Rev Endocrinol. 2022;18(4):243–58.
15. Sun N, Youle RJ, Finkel T. The mitochondrial basis of aging. Mol Cell. 2016;61(5):654–66.
16. Detmer SA, Chan DC. Functions and dysfunctions of mitochondrial dynamics. Nat Rev Mol Cell Biol. 2007;8(11):870–9.
17. Chakrabarty RP, Chandel NS. Mitochondria as Signaling Organelles Control mammalian stem cell fate. Cell Stem Cell. 2021;28(3):394–408.
18. Wallace DC. Mitochondrial genetic medicine. Nat Genet. 2018;50(12):1642–9.
19. Kim J, Gupta R, Blanco LP, Yang S, Shteinfer-Kuzmine A, Wang K, Zhu J, Yoon HE, Wang X, Kerkhofs M, Kang H, Brown AL, Park SJ, Xu X, van Zandee E, Kim MK, Cohen JI, Kaplan MJ, Shoshan-Barmatz V, Chung JH. VDAC oligomers form mitochondrial pores to release mtDNA fragments and promote lupus-like disease. Sci (New York N Y). 2019;366(6472):1531–6.
20. Victorelli S, Salmonowicz H, Chapman J, Martini H, Vizioli MG, Riley JS, Cloix C, Hall-Younger E, Machado Espindola-Netto J, Jurk D, Lagnado AB, Sales Gomez L, Farr JN, Saul D, Reed R, Kelly G, Eppard M, Greaves LC, Dou Z, Pirius N, Szczepanowska K, Porritt RA, Huang H, Huang TY, Mann DA, Masuda CA, Khosla S, Dai H, Kaufmann SH, Zacharioudakis E, Gavathiotis E, LeBrasseur NK, Lei X, Sainz AG, Korolchuk VI, Adams PD, Shadel GS, Tait S W. G.;, Passos. J. F., Apoptotic stress causes mtDNA release during senescence and drives the SASP. *Nature* 2023, *622* (7983), 627–636.
21. West AP, Khoury-Hanold W, Staron M, Tal MC, Pineda CM, Lang SM, Bestwick M, Duguay BA, Raimundo N, MacDuff DA, Kaech SM, Smiley JR, Means RE, Iwasaki A, Shadel GS. Mitochondrial DNA stress primes the antiviral innate immune response. Nature. 2015;520(7548):553–7.
22. Salminen A, Ojala J, Kaarniranta K. Apoptosis and aging: increased resistance to apoptosis enhances the aging process. Cell Mol Life Sci. 2011;68(6):1021–31.
23. Bazhanova ED, Anisimov VN. [FAS- and TNF-dependent ways participation in apoptosis mechanisms in hypotalumus in physiological and pathological aging]. Adv Gerontol. 2020;33(1):34–9.
24. Nakamura-López Y, Sarmiento-Silva RE, Moran-Andrade J, Gómez-García B. Staurosporine-induced apoptosis in P388D1 macrophages involves both extrinsic and intrinsic pathways. Cell Biol Int. 2009;33(9):1026–31.
25. Jauhari A, Baranov SV, Suofu Y, Kim J, Singh T, Yablonska S, Li F, Wang X, Oberly P, Minnigh MB, Poloyac SM, Carlisle DL, Friedlander RM. Melatonin inhibits cytosolic mitochondrial DNA-induced neuroinflammatory signaling in accelerated aging and neurodegeneration. J Clin Invest. 2020;130(6):3124–36.

26. Lopez-Otin C, Blasco MA, Partridge L, Serrano M, Kroemer G. Hallmarks of aging: an expanding universe. Cell. 2023;186(2):243–78.
27. Miwa S, Kashyap S, Chini E, von Zglinicki T. Mitochondrial dysfunction in cell senescence and aging. J Clin Invest. 2022;132:13.
28. Kenny TC, Khan A, Son Y, Yue L, Heissel S, Sharma A, Pasolli HA, Liu Y, Gamazon ER, Alwaseem H, Hite RK, Birsoy K. Integrative genetic analysis identifies FLVCR1 as a plasma-membrane choline transporter in mammals. Cell Metab. 2023;35(6):1057–71. e12.
29. Calo E, Gu B, Bowen ME, Aryan F, Zalc A, Liang J, Flynn RA, Swigut T, Chang HY, Attardi LD, Wysocka J. Tissue-selective effects of nucleolar stress and rDNA damage in developmental disorders. Nature. 2018;554(7690):112–7.
30. Werner A, Iwasaki S, McGourty CA, Medina-Ruiz S, Teerikorpi N, Fedrigo I, Ingolia NT, Rape M. Cell-fate determination by ubiquitin-dependent regulation of translation. Nature. 2015;525(7570):523–7.
31. Hou Y, Dan X, Babbar M, Wei Y, Hasselbalch SG, Croteau DL, Bohr VA. Ageing as a risk factor for neurodegenerative disease. Nat Reviews Neurol. 2019;15(10):565–81.
32. Stern Y. Cognitive reserve in ageing and Alzheimer's disease. Lancet Neurol. 2012;11(11):1006–12.
33. Doolittle ML, Saul D, Kaur J, Rowsey JL, Vos SJ, Pavelko KD, Farr JN, Monroe DG, Khosla S. Multiparametric senescent cell phenotyping reveals targets of senolytic therapy in the aged murine skeleton. Nat Commun. 2023;14(1):4587.
34. López-Otín C, Blasco MA, Partridge L, Serrano M, Kroemer G. The hallmarks of aging. Cell. 2013;153(6):1194–217.
35. Pouikli A, Parekh S, Maleszewska M, Nikopoulou C, Baghdadi M, Tripodi I, Folz-Donahue K, Hinze Y, Mesaros A, Hoey D, Giavalisco P, Dowell R, Partridge L, Tessarz P. Chromatin remodeling due to degradation of citrate carrier impairs osteogenesis of aged mesenchymal stem cells. Nat Aging. 2021;1(9):810–25.
36. Argüelles S, Guerrero-Castilla A, Cano M, Muñoz MF, Ayala A. Advantages and disadvantages of apoptosis in the aging process. Ann N Y Acad Sci. 2019;1443(1):20–33.
37. Tower J. Programmed cell death in aging. Ageing Res Rev. 2015;23(Pt A):90–100.
38. Li X, Li C, Zhang W, Wang Y, Qian P, Huang H. Inflammation and aging: signaling pathways and intervention therapies. Signal Transduct Target Therapy. 2023;8(1):239.
39. López-Otín C, Blasco MA, Partridge L, Serrano M, Kroemer G. Hallmarks of aging: an expanding universe. Cell. 2023;186(2):243–78.
40. Anderson CJ, Medina CB, Barron BJ, Karvelyte L, Aaes TL, Lambertz I, Perry JSA, Mehrotra P, Gonçalves A, Lemeire K, Blancke G, Andries V, Ghazavi F, Martens A, van Loo G, Vereecke L, Vandenabeele P, Ravichandran KS. Microbes exploit death-induced nutrient release by gut epithelial cells. Nature. 2021;596(7871):262–7.
41. Sfeir JG, Drake MT, Khosla S, Farr JN. Skeletal Aging. *Mayo Clinic proceedings* 2022, *97* (6), 1194–1208.
42. Farr JN, Xu M, Weivoda MM, Monroe DG, Fraser DG, Onken JL, Negley BA, Sfeir JG, Ogrodnik MB, Hachfeld CM, LeBrasseur NK, Drake MT, Pignolo RJ, Pirtskhalava T, Tchkonia T, Oursler MJ, Kirkland JL, Khosla S. Targeting cellular senescence prevents age-related bone loss in mice. Nat Med. 2017;23(9):1072–9.
43. Novais EJ, Tran VA, Johnston SN, Darris KR, Roupas AJ, Sessions GA, Shapiro IM, Diekman BO, Risbud MV. Long-term treatment with senolytic drugs Dasatinib and Quercetin ameliorates age-dependent intervertebral disc degeneration in mice. Nat Commun. 2021;12(1):5213.
44. Arandjelovic S, Ravichandran KS. Phagocytosis of apoptotic cells in homeostasis. Nat Immunol. 2015;16(9):907–17.
45. Yáñez-Mó M, Siljander PR, Andreu Z, Zavec AB, Borràs FE, Buzas EI, Buzas K, Casal E, Cappello F, Carvalho J, Colás E, Cordeiro-da Silva A, Fais S, Falcon-Perez JM, Ghobrial IM, Giebel B, Gimona M, Graner M, Gursel I, Gursel M, Heegaard NH, Hendrix A, Kierulf P, Kokubun K, Kosanovic M, Kralj-Iglic V, Krämer-Albers EM, Laitinen S, Lässer C, Lener T, Ligeti E, Linē A, Lipps G, Llorente A, Lötvall J, Manček-Keber M, Marcilla A, Mittelbrunn M, Nazarenko I, Nolte TA, O'Driscoll L, Olivan M, Oliveira C, Pállinger É, Del Portillo HA, Reventós J, Rigau M, Rohde E, Sammar M, Sánchez-Madrid F, Santarém N, Schallmoser K, Ostenfeld MS, Stoorvogel W, Stukelj R, Van der Grein SG, Vasconcelos MH, Wauben M. H.; De Wever, O., Biological properties of extracellular vesicles and their physiological functions. *Journal of extracellular vesicles* 2015, *4*, 27066.
46. Lötvall J, Hill AF, Hochberg F, Buzás EI, Di Vizio D, Gardiner C, Gho YS, Kurochkin IV, Mathivanan S, Quesenberry P, Sahoo S, Tahara H, Wauben MH, Witwer KW, Théry C. Minimal experimental requirements for definition of extracellular vesicles and their functions: a position statement from the International Society for Extracellular Vesicles. J Extracell Vesicles. 2014;3:26913.
47. Akers JC, Gonda D, Kim R, Carter BS, Chen CC. Biogenesis of extracellular vesicles (EV): exosomes, microvesicles, retrovirus-like vesicles, and apoptotic bodies. J Neurooncol. 2013;113(1):1–11.
48. Zhang X, Tang J, Kou X, Huang W, Zhu Y, Jiang Y, Yang K, Li C, Hao M, Qu Y, Ma L, Chen C, Shi S, Zhou Y. Proteomic analysis of MSC-derived apoptotic vesicles identifies Fas inheritance to ameliorate haemophilia a via activating platelet functions. 2022, *11* (7), 11:e12240.
49. Evans MJ, Kaufman MH. Establishment in culture of pluripotential cells from mouse embryos. Nature. 1981;292(5819):154–6.
50. Huang G, Ye S, Zhou X, Liu D, Ying QL. Molecular basis of embryonic stem cell self-renewal: from signaling pathways to pluripotency network. Cell Mol Life Sci. 2015;72(9):1741–57.
51. Solter D, Gearhart J. Putting stem cells to work. Sci (New York N Y). 1999;283(5407):1468–70.
52. Le Blanc K, Tammik L, Sundberg B, Haynesworth SE, Ringdén O. Mesenchymal stem cells inhibit and stimulate mixed lymphocyte cultures and mitogenic responses independently of the major histocompatibility complex. Scand J Immunol. 2003;57(1):11–20.
53. Le Blanc K, Tammik C, Rosendahl K, Zetterberg E, Ringdén O. HLA expression and immunologic properties of differentiated and undifferentiated mesenchymal stem cells. Exp Hematol. 2003;31(10):890–6.
54. Zhunina OA, Yabbarov NG, Grechko AV, Starodubova AV, Ivanova E, Nikiforov NG, Orekhov AN. The role of mitochondrial dysfunction in Vascular Disease, Tumorigenesis, and diabetes. Front Mol Biosci. 2021;8:671908.
55. Passos JF, Saretzki G, Ahmed S, Nelson G, Richter T, Peters H, Wappler I, Birket MJ, Harold G, Schaeuble K, Birch-Machin MA, Kirkwood TB, von Zglinicki T. Mitochondrial dysfunction accounts for the stochastic heterogeneity in telomere-dependent senescence. PLoS Biol 2007, 5 (5), e110.
56. Passos JF, Nelson G, Wang C, Richter T, Simillion C, Proctor CJ, Miwa S, Olijslagers S, Hallinan J, Wipat A, Saretzki G, Rudolph KL, Kirkwood TB, von Zglinicki T. Feedback between p21 and reactive oxygen production is necessary for cell senescence. Mol Syst Biol. 2010;6:347.
57. Nelson G, Kucheryavenko O, Wordsworth J, von Zglinicki T. The senescent bystander effect is caused by ROS-activated NF-κB signalling. Mech Ageing Dev. 2018;170:30–6.
58. Di Micco R, Fumagalli M, Cicalese A, Piccinin S, Gasparini P, Luise C, Schurra C, Garre M, Nuciforo PG, Bensimon A, Maestro R, Pelicci PG, Fagagna F. Oncogene-induced senescence is a DNA damage response triggered by DNA hyper-replication. Nature. 2006;444(7119):638–42.
59. Correia-Melo C, Marques FD, Anderson R, Hewitt G, Hewitt R, Cole J, Carroll BM, Miwa S, Birch J, Merz A, Rushton MD, Charles M, Jurk D, Tait SW, Czapiewski R, Greaves L, Nelson G, Bohlooly YM, Rodriguez-Cuenca S, Vidal-Puig A, Mann D, Saretzki G, Quarato G, Green DR, Adams PD, von Zglinicki T, Korolchuk VI, Passos JF. Mitochondria are required for pro-ageing features of the senescent phenotype. Embo j. 2016;35(7):724–42.
60. Gluck S, Guey B, Gulen MF, Wolter K, Kang TW, Schmacke NA, Bridgeman A, Rehwinkel J, Zender L, Ablasser A. Innate immune sensing of cytosolic chromatin fragments through cGAS promotes senescence. Nat Cell Biol. 2017;19(9):1061–70.
61. Positional cloning of. A gene involved in the pathogenesis of Treacher Collins syndrome. The Treacher Collins Syndrome Collaborative Group. Nat Genet. 1996;12(2):130–6.
62. Valdez BC, Henning D, So RB, Dixon J, Dixon MJ. The Treacher Collins syndrome (TCOF1) gene product is involved in ribosomal DNA gene transcription by interacting with upstream binding factor. Proc Natl Acad Sci USA. 2004;101(29):10709–14.
63. Dixon J, Jones NC, Sandell LL, Jayasinghe SM, Crane J, Rey JP, Dixon MJ, Trainor PA. Tcof1/Treacle is required for neural crest cell formation and proliferation deficiencies that cause craniofacial abnormalities. Proc Natl Acad Sci USA. 2006;103(36):13403–8.
64. Sakai D, Dixon J, Dixon MJ, Trainor PA. Mammalian neurogenesis requires Treacle-Plk1 for precise control of spindle orientation, mitotic progression, and maintenance of neural progenitor cells. PLoS Genet 2012, 8 (3), e1002566.
65. Sakai D, Trainor PA. Face off against ROS: Tcof1/Treacle safeguards neuroepithelial cells and progenitor neural crest cells from oxidative stress during craniofacial development. Dev Growth Differ. 2016;58(7):577–85.
66. Omori S, Wang TW, Johmura Y, Kanai T, Nakano Y, Kido T, Susaki EA, Nakajima T, Shichino S, Ueha S, Ozawa M, Yokote K, Kumamoto S, Nishiyama A, Sakamoto T, Yamaguchi K, Hatakeyama S, Shimizu E, Katayama K, Yamada

Y, Yamazaki S, Iwasaki K, Miyoshi C, Funato H, Yanagisawa M, Ueno H, Imoto S, Furukawa Y, Yoshida N, Matsushima K, Ueda HR, Miyajima A, Nakanishi M. Generation of a p16 reporter mouse and its use to characterize and target p16(high) cells in vivo. Cell Metab. 2020;32(5):814–e8286.

67. He B, Yu H, Liu S, Wan H, Fu S, Liu S, Yang J, Zhang Z, Huang H, Li Q, Wang F, Jiang Z, Liu Q, Jiang H. Mitochondrial cristae architecture protects against mtDNA release and inflammation. Cell Rep. 2022;41(10):111774.

Publisher's note